Journal of Power Sources 218 (2012) 268–279

Contents lists available at SciVerse ScienceDirect

Journal of Power Sources

journal homepage: www.elsevier.com/locate/jpowsour

Modeling and optimization of the DMFC system: Relating materials properties to system size and performance

Brent Bennett*, Babar M. Koraishy, Jeremy P. Meyers [1]

Department of Mechanical Engineering, The Center for Electrochemistry, The University of Texas at Austin, 1 University Station, C2200, Austin, TX 78712-0292, USA

HIGHLIGHTS

- ► Analytic model of oxygen concentration in the direct methanol fuel cell.
- ► Fuel cell power output is compared to power consumption of system components.
- ► Performance of new membrane materials is compared to that of Nafion.
- ► Optimum flow rates are suggested for a variety of materials and system parameters.

ARTICLE INFO

Article history:
Received 29 April 2012
Received in revised form
26 June 2012
Accepted 28 June 2012
Available online 5 July 2012

Keywords:
Direct methanol fuel cell (DMFC) model
Methanol crossover
DMFC performance
DMFC efficiency
DMFC system design

ABSTRACT

In designing a direct methanol fuel cell and evaluating the appropriateness of new materials for inclusion, it is helpful to consider the impact of material properties on the performance of a complete system: to some degree, poor fuel utilization and performance losses from methanol crossover can be mitigated by proper system design. Simple engineering models can be useful tools in facilitating this type of system design. In this paper, an analytical model is developed to determine the oxygen concentration profile in the cathode backing layer and flow channel along a one-dimensional cross-section of the fuel cell. An existing analytical model is then used to determine the methanol concentration profile in the anode backing layer and membrane and the methanol crossover current along the same cross-section. Applying a fixed cell potential and using Tafel kinetics to describe the charge-transfer reactions at the anode and the cathode, the local current density and the rates of methanol and oxygen consumption are determined. The process repeats for a fixed number of cross-sections down the entire length of the flow channels, and the average current density and stoichiometric ratios are calculated at the end. The model is applied to examine the effects of new low-crossover membranes and to suggest new design parameters for those membranes. Also, an analysis is presented in which the tradeoff between stack power and the size of system components is examined for a range of methanol and oxygen flow rates.

1. Introduction

The direct methanol fuel cell (DMFC) is an electrochemical energy conversion device that operates by converting methanol and water to carbon dioxide and protons at the anode, $CH_3OH + H_2O \rightleftharpoons CO_2 + 6H^+ + 6e^-$, and by reducing oxygen at the cathode, $O_2 + 4H^+ + 4e^- \rightleftharpoons 2H_2O$. The primary advantage of the DMFC is that it can be operated with a liquid anode feed and therefore does not require a reformer or a bulky gas storage tank. Also, because the oxidation reaction produces six electrons per methanol molecule, the DMFC delivers a high specific energy. The simplicity and compactness of the fuel delivery system makes the DMFC attractive for portable applications.

A paramount problem in the implementation of the DMFC is methanol crossing over to the cathode, where it is oxidized, resulting in depolarization of the positive electrode and wasted fuel. The origin of crossover lies in the fact that methanol is completely soluble in water and that water is needed to swell the proton-exchange membrane and to impart protonic conductivity across the membrane. One way to mitigate this problem is to create a low-crossover membrane to replace standard perfluorosulfonic acid membranes such as Nafion®. Increasing the efficiency of the reactions at the anode and the cathode through the design of the catalyst layers can also minimize the harmful effects of crossover.

* Corresponding author. Tel.: +1 432 528 0899; fax: +1 512 471 1045.
E-mail address: brent.bennett@utexas.edu (B. Bennett).
[1] Present address: EnerVault Corporation, 1244 Reamwood Avenue, Sunnyvale, CA 94089, USA.

0378-7753/$ – see front matter © 2012 Elsevier B.V. All rights reserved.
http://dx.doi.org/10.1016/j.jpowsour.2012.06.095

Finally, it is important to optimize the design of the flow channels and operating parameters such as the methanol and oxygen feed concentrations and the temperature.

During the past two decades, numerous approaches to modeling the DMFC have been taken. Most of these models focus on specific aspects of the fuel cell, such as polarization, multiphase transport, or methanol crossover. In the majority of the models, fuel utilization, system efficiency and other system-level engineering problems, if considered at all, is only given brief discussion. However, there are still many DMFC models in the literature that focus explicitly on issues such as fuel utilization [1–7], system efficiency [8,9], optimization of methanol and oxygen flow throughout the fuel cell stack [10–14], exergy and thermal analyses [14–17], and system size and cost [11,16,18]. What most of these models lack are simple connections among materials properties, operating parameters, and system constraints.

This work seeks to make those connections by incorporating as many analytic expressions as possible. Specifically, the goal here is to examine the effect of materials properties, especially properties relating to the proton-exchange membrane, on the net power output and total size of the fuel cell system. System size is a critical factor for the cost and portability for small DMFCs. Running at high utilization rates (low flow rates) will lower the size of the system components such as the methanol tank and the air blower but will reduce performance and require a larger fuel cell stack to achieve a certain power output. Conversely, running at low utilization rates (high flow rates) will increase power output and reduce the stack size but will require a larger methanol tank and air blower. To perform this analysis, we designed a model that incorporates as many analytic solutions as possible for simple use and fast run times in a MATLAB simulation environment.

To create the desired model, we seek to derive analytical solutions for the methanol and oxygen concentration profiles along a single one-dimensional cross-section of the fuel cell. The solutions for the methanol concentration in the anode backing layer and membrane taken from our previous publication [11]. Similar equations are derived in this work for the oxygen concentration in the cathode backing layer and flow channel. We then apply Tafel kinetics with a fixed cell potential to determine the local current density and the consumption of methanol and oxygen reactants along a single cross-section of the cell. Using a forward difference approach, the methanol and oxygen concentrations at the next point in the flow channel are calculated. The model is stepped down the flow channels in this manner, and the average current density is calculated by dividing the sum of all the cross-sectional currents by the number of steps.

In the first part of the analysis, we simulate polarization data for a cell operating at fixed inlet concentrations and flow rates of methanol and oxygen. In order to validate the model, we compare the model's predictions with experimental data for the performance of DMFCs running at low utilization rates of both oxygen and air at 65 °C and 90 °C. This data provides a base case for setting the standard kinetic parameters in the model, such as the exchange current densities and the symmetry coefficients. We then apply the model to anticipate the effects of using new low-crossover membranes from Zhu et al. on fuel cell performance, and we offer suggestions on how to design and operate fuel cells that use the new membranes.

In the second part of the analysis, we consider the system-level tradeoff between the power output of the cell and the size of the methanol storage tank and air blower. We set a desired current output for the cell (50 mA cm^{-2} or 300 mA cm^{-2}) and calculate the power output at different oxygen and methanol flow rates and methanol concentrations. We also consider the system-level benefits of using the new membranes. The size of the methanol tank and the air blower should scale linearly with the flow rates while the marginal increase in power output will diminish as the flow rates increase. Therefore, given a set of performance constraints, we expect to find flow rates that minimize the total size of the fuel stack in combination with the other system components.

2. Model development

2.1. Assumptions

In Section 2.1, we develop analytic solutions for the oxygen concentration in the cathode backing layer and across the thickness of the cathode flow channel. For the analytic solutions of the methanol concentration profile in the anode backing layer and in the membrane, we again refer the reader to our previous publication [4]. The notation from that publication is carried into this work. Section 2.2 shows how the local current density is found using the Tafel equations and assuming a constant cell voltage. In Section 2.3, we use the local current density to calculate the local methanol and oxygen consumption in the flow channels and then apply a forward difference method to determine the methanol and oxygen concentration profiles down the entire length of the channels. At the end, the stoichiometric coefficients are calculated using the average current density in the fuel cell.

In the development of the model that follows, we assume that all fluxes and current densities are defined per unit of superficial area, and transport properties in the backing layers and membrane are effective transport properties, modified from bulk values by appropriate corrections for volume fraction and tortuosity. The term "current" will always refer to the specific current density unless otherwise noted. We also neglect convection across the thickness of the cell. The methanol flux across the cell is dominated by diffusion in the anode backing layer and is a combination of diffusion and electroosmotic drag in the membrane, while the oxygen flux is due solely to convection in the flow channel and molecular diffusion in the cathode backing layer. The methanol concentration is driven to zero at the boundary between the membrane and the cathode backing layer, whereas the oxygen partial pressure maintains a finite value at that same boundary (Fig. 1).

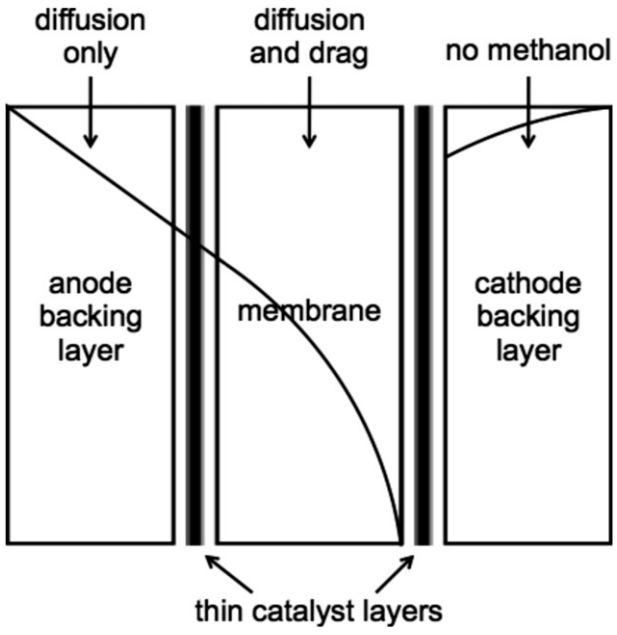

Fig. 1. Cross-section of the cell including a qualitative rendering of the methanol and oxygen concentration profiles.

The most critical assumption in this model is that any effects stemming from water transport or carbon dioxide gas removal are ignored or incorporated into effective diffusion coefficients. This assumption allows for analytic solutions for the oxygen concentration to be developed, but it also restricts the validity of the model to low-power applications. In systems using high current density and high methanol concentration (above 2 M), or in any scenario where water flux in the cathode and carbon dioxide generation in the anode and cathode are substantial, the model's ability to provide accurate performance predictions is limited. However, in applications such as portable communications, where system efficiency and system size are paramount, the fuel cell is often operated at low current densities. These systems need to run lean on fuel in order to carry the methanol oxidation reaction to completion, thereby avoiding wasted fuel and the production of intermediaries. In these low-power systems, the model should have a wide range of applicability.

Another important simplification is the assumption of Tafel kinetics for both methanol oxidation and oxygen reduction. Both reactions are multi-step, and Tafel kinetics only applies to the rate-determining step in each case. However, in the cases described here, the exchange current densities for both reactions, $\sim 10^{-5}$ for methanol oxidation and $\sim 10^{-7}$ for oxygen reduction, are at least two orders of magnitude below the cell current density, which ranges from about 1 mA cm^{-2} to 1 A cm^{-2} in the experimental data used to verify the model. Therefore, the reaction is forward-biased to such an extent that we can assume the intermediate steps proceed rapidly and apply the Tafel equation to the rate-determining step. As long as the current density is not so high that adsorption of the reactants on the catalyst sites becomes rate-determining, Tafel kinetics should be sufficient to describe the entirety of the electrode reactions. See, for example, an analysis of methanol reaction kinetics under relevant conditions in Ref. [26].

The methanol solution is assumed to be an ideal incompressible liquid in an isothermal environment such that any pressure or local temperature effects can also be ignored. The air in the cathode is assumed to be an ideal gas, and only water in the vapor phase is considered explicitly at the cathode. Much work has been done, most notably by Scott et al. [19] and by Wang and Wang [20], to show that two-phase effects at the anode can be important even in liquid-feed DMFCs, but this model does not consider those effects. Instead, we assume that the behavior of the backing layers can be characterized simply by an effective diffusion coefficient and by their thickness.

$$P_{H_2O,sat} = \exp\left[11.6832 - \frac{3816.44}{(T - 46.13)}\right], \tag{1}$$

then the oxygen partial pressure will be 20.946% of the remaining total pressure for an air feed. A study by Weber and Newman [22] confirms that when the cathode backing layer in a PEM fuel cell has a high porosity and a relatively small pressure gradient across it, convection and Knudsen diffusion can be safely ignored. Therefore, in order to obtain an analytic solution of the oxygen concentration profile across the backing layer, we use Stefan–Maxwell diffusion to fully describe the transport of oxygen in that region

$$\frac{P_{total}}{RT}\frac{\partial y_{O_2}^{back}}{\partial x} = \left(-\frac{y_{N_2}}{D_{O_2-N_2}^{eff}} - \frac{y_{H_2O}}{D_{O_2-H_2O}^{eff}}\right) N_{O_2}^{back} + \left(\frac{y_{O_2}}{D_{O_2-N_2}^{eff}}\right) N_{N_2}^{back} + \left(\frac{y_{O_2}}{D_{O_2-H_2O}^{eff}}\right) N_{H_2O}^{back}. \tag{2}$$

Again note that $D_{O_2-N_2}^{eff}$ and $D_{O_2-H_2O}^{eff}$ are *effective* diffusion coefficients for the components in the porous backing layer. The flux of water and nitrogen across the backing layer is negligible, allowing us to ignore the last two terms. Substituting partial pressures for the mole fractions and $N_{O_2}^{back} = (i + i_x)/4F$ for the oxygen flux, we find an expression for the change in absolute oxygen pressure across the backing layer

$$\frac{\partial P_{O_2}^{back}}{\partial x} = \frac{RT}{P_{total}}\left(-\frac{P_{N_2}}{D_{O_2-N_2}^{eff}} - \frac{P_{H_2O}}{D_{O_2-H_2O}^{eff}}\right)\left(\frac{i + i_x}{4F}\right), \tag{3}$$

where $P_{total} = P_{O_2}^{back} + P_{N_2} + P_{H_2O}$ with P_{N_2} and P_{H_2O} constant. P_{H_2O} is always set to the saturated value because there is assumed to be some liquid water in the cathode backing layer at all times, and P_{N_2} is either 79.054% of the remaining total pressure for an air feed or zero for an oxygen feed.

Since $P_{O_2}^{back}$ is included in P_{total}, it is now on both sides of this equation, which means that the pressure profile in the backing layer is nonlinear. The appropriate boundary conditions are $P_{O_2}^{back} = P_{O_2,s}$ at $x = 0$ and $P_{O_2}^{back} = P_{O_2,c}$ at $x = L_{back,c}$, where $P_{O_2,s}$ is the oxygen pressure at the boundary between the backing layer and the flow channel and $P_{O_2,c}$ is the oxygen pressure at the boundary between the membrane and the backing layer. After integrating with these boundary conditions, we find the expression

$$P_{O_2,c} = -(P_{N_2} + P_{H_2O}) + \sqrt{(P_{O_2,s} + P_{N_2} + P_{H_2O})^2 - 2(i + i_x)\left(\frac{RT}{4F}\right)\left(\frac{P_{N_2}}{D_{O_2-N_2}^{eff}} + \frac{P_{H_2O}}{D_{O_2-H_2O}^{eff}}\right)L_{back,c}}. \tag{4}$$

2.2. Oxygen pressure in the cathode

2.2.1. Cathode backing layer

In the cathode, we assume that the incoming air stream is a pure mixture of oxygen, nitrogen (if air is used instead of pure oxygen), and water vapor (if humidified). If we assume that cathode feed stream obeys the ideal gas law, then $c_{O_2} = P_{O_2}/RT$, where $P_{O_2} = y_{O_2}P_{total}$ is the absolute oxygen pressure. We again emphasize that the effects of any liquid water present in the backing layer or the flow channel are incorporated into the effective diffusion coefficients. If the feed stream is humidified and if the saturation vapor pressure of water is solely a function of temperature [21]

2.2.2. Oxygen transport from cathode flow channel to backing layer

A crucial difference between the treatment of the anode and the cathode is the need to consider the movement of oxygen gas from the bulk of the flow channel to the surface of the cathode backing layer. The change in oxygen partial pressure across this distance takes the same form as Eq. (3)

$$\frac{\partial P_{O_2}^{conv}}{\partial x} = \frac{RT}{P_{total}}\left(-\frac{P_{N_2}}{D_{O_2-N_2}} - \frac{P_{H_2O}}{D_{O_2-H_2O}}\right)\left(\frac{i + i_x}{4F}\right), \tag{5}$$

where $P_{O_2}^{conv}$ is the absolute oxygen pressure in the convective region between the bulk flow channel and the backing layer surface. Note that the diffusion coefficients lack the eff

subscript because we are outside the porous region of the backing layer.

As with $P_{O_2}^{back}$, $P_{O_2}^{conv}$ is included in P_{total} and is on both sides of Eq. (5), so the result is a nonlinear pressure profile. The appropriate boundary conditions are $P_{O_2}^{conv} = P_{O_2,f}$ at $x = 0$ and $P_{O_2}^{conv} = P_{O_2,s}$ at $x = d_h/Sh_F$, i.e. the backing layer surface, where d_h is the hydraulic diameter of the channel and $Sh_F = 2.71$ is the Sherwood number for a square channel [23]. $P_{O_2,f}$ is the oxygen pressure in the bulk flow channel and is determined according to the solution method given in Section 2.4.2. Integrating Eq. (5) with these boundary conditions results in an expression for the oxygen pressure at the surface of the cathode baking layer that is almost identical in form to the expression for $P_{O_2,c}$.

$$P_{O_2,s} = -(P_{N_2} + P_{H_2O}) + \sqrt{\left(P_{O_2,f} + P_{N_2} + P_{H_2O}\right)^2 - 2(i + i_x)\left(\frac{RT}{4F}\right)\left(\frac{P_{N_2}}{D_{O_2-N_2}} + \frac{P_{H_2O}}{D_{O_2-H_2O}}\right)\frac{d_h}{Sh_F}}. \quad (6)$$

We then substitute $P_{O_2,s}$ directly into Eq. … to obtain the following expression for $P_{O_2,c}$ terms of $P_{O_2,f}$

$$P_{O_2,c} = -(P_{N_2} + P_{H_2O}) + \sqrt{\left(P_{O_2,f} + P_{N_2} + P_{H_2O}\right)^2 - 2(i + i_x)\left(\frac{RT}{4F}\right)\left[\left(\frac{P_{N_2}}{D_{O_2-N_2}} + \frac{P_{H_2O}}{D_{O_2-H_2O}}\right)\frac{d_h}{Sh_F} + \left(\frac{P_{N_2}}{D_{O_2-N_2}^{eff}} + \frac{P_{H_2O}}{D_{O_2-H_2O}^{eff}}\right)L_{back,c}\right]}. \quad (7)$$

The resulting expression cannot be simplified and must be substituted in this form when we solve for the desired current i. Aside from i, the other unknown in Eq. (7) is the oxygen pressure in the bulk flow channel $P_{O_2,f}$. The solution methods for i and $P_{O_2,f}$ are described in Sections 2.2 and 2.3.2.

2.2.3. Oxygen transport in the cathode catalyst layer

While maintaining the assumption of thin catalyst layers, we will choose to define an effectiveness factor to account for the mass transport of oxygen in the cathode catalyst layer because the oxygen reduction reaction is first-order. The methanol oxidation reaction is still assumed to be zero-order, so there is no need to define an effectiveness factor there. The effectiveness factor is a dimensionless quantity that relates the actual rate of reaction to the rate if the entire interior of the catalyst layer was exposed to the conditions that exist at the catalyst layer/backing layer boundary. In effect, it is a measure of how far into the catalyst layer the oxygen penetrates and is a simpler and more convenient method of accounting for mass transport in the catalyst layer than applying a full model containing terms for molecular diffusion, Knudsen diffusion (particularly important in catalyst layers and microporous layers), and convection.

Assuming Tafel kinetics, at steady-state the governing equation for the material balance of oxygen in the catalyst layer is [1]

$$\frac{d^2c(x)}{dx^2} - \frac{i_c^0}{4FL_{cl}D_{O_2,cl}^{eff}}\frac{RT}{P_{O_2,c}}\exp\left[-\frac{\alpha_c F}{RT}(V_{cathode})\right]c(x) = 0. \quad (8)$$

where i_c^0 is the exchange current density in A cm^{-2}, L_{cl} is the catalyst layer thickness, $P_{O_2,c}$ is the oxygen pressure at the catalyst layer surface, α_c is the cathodic transfer coefficient, and $V_{cathode}$ is the cathodic activation overpotential. Because of the complexity of oxygen diffusion in the catalyst layer, which has relatively low porosity and high water saturation, we choose to use an effective diffusion coefficient of oxygen $D_{O_2,cl}^{eff}$ based on the idea that the catalyst layer is fully flooded and that the diffusion of oxygen only occurs in the regions containing Nafion [24]

$$D_{O_2,cl}^{eff} = D_{O_2,Nafion}\left[(1 - \varepsilon_{cl})\phi_{Nafion}\right]^{1.5}. \quad (9)$$

where $D_{O_2,Nafion} = 5.23 \times 10^{-6}\exp[(23849/R)*((1/333.15) - (1/T))]$cm^2 s^{-1} [25], ε_{cl} is the porosity of the catalyst layer, and ϕ_{Nafion} is the volume fraction of Nafion in the catalyst layer. Making the governing equation dimensionless leads us to define the Thiele modulus as follows [1]:

$$\theta^2 = \frac{i_c^0 L_{cl}}{4FD_{O_2,cl}^{eff}}\frac{RT}{P_{O_2,c}}\exp\left[-\frac{\alpha_c F}{RT}(V_{cathode})\right]. \quad (10)$$

Subsequently, the effectiveness factor is a function of the Thiele modulus: $\eta = (\tanh\theta)/\theta$. For an effectiveness factor close to unity, internal mass transport in the catalyst layer is minimal, and the reactant penetrates fully into the catalyst layer. If the effectiveness factor is closer to zero, mass transport in the catalyst layer is a significant issue, and the catalyst layer is not being fully utilized. In DMFC cathodes the effectiveness factor is much less of an issue than in PEMFCs due to lower operating current densities. Even with the relatively thick cathode catalyst layer in this model ($L_{cl} = 10$ μm), the effectiveness factor is rarely below 0.9. However, because including it does not add noticeably to the computation time, we choose to include it for the sake of completeness and accuracy.

2.3. Overpotentials and current solution method

2.3.1. Determination of overpotentials and cell potential

Now that the concentration profiles for methanol and oxygen have been developed for a one-dimensional cross-section of the cell in terms of the desired current i, all that remains is to solve for that current. As stated in the introduction, our strategy is to assume the cell potential remains constant and numerically solve for the local current along each cross-section. Given the high in-plane conductivity of the bipolar plates, any voltage difference along the plates will be quickly dissipated, so the assumption of a constant cell potential appears reasonable. The cell potential is defined as follows:

$$V_{cell} = U^\theta - i\frac{L_{mem}}{\kappa_{mem}} - \frac{i}{2}\left(\frac{L_{cla}}{\kappa_{cla}} + \frac{L_{clc}}{\kappa_{clc}}\right) - V_{anode} + V_{cathode}, \quad (11)$$

where κ_{mem} is the membrane conductivity in S cm^{-1}, κ_{cla} and κ_{clc} are the anode and cathode catalyst layer conductivity in S cm^{-1} and $U^{\theta} = 1.21$ V for the DMFC. Implicit in this equation is the assumption that the proton conductivity is uniform throughout the thickness of the catalyst layers and the membrane. While each is tracked separately, and preserves the ability to describe restricted proton access in the catalyst layers, where the volume fraction of ionomer is lower than in the membrane separator, we do neglect the possibility of variation through the thickness of any of the components. Furthermore, the factor of ½ appears in front of the catalyst layer ohmic terms because we assume that the protons travel on average half the distance across each catalyst layer. While this assumption is not true in a situation where there are substantial mass-transport limitations in the catalyst layers, zero-order kinetics at the anode and an effectiveness factor that is almost always above 0.9 at the cathode support the notion that the reactions are occurring somewhat uniformly across the catalyst layers.

As mentioned previously, both the methanol oxidation and oxygen reduction reactions are assumed to follow Tafel kinetics, with the former being zero-order and the later being first-order. The assumption of zero-order kinetics has been shown to be accurate to very low concentrations or operation very near the limiting current, and is tantamount to assuming that the CO-sites on the anode electrocatalyst can quickly become saturated [26].

$$V_{anode} = \frac{RT}{F\alpha_a}\ln\left(\frac{i}{i_a^0}\right) \tag{12}$$

$$V_{cathode} = \frac{RT}{F\alpha_c}\ln\left(\eta\frac{P_{O_2,c}}{P_{O_2,ref}}\frac{i_c^0}{i+i_x}\right) \tag{13}$$

Note the presence of the effectiveness factor in the cathodic overpotential. Maintaining zero-order methanol kinetics means that the anode overpotential does not depend on the methanol concentration at the anode catalyst layer. This assumption is valid as long as we keep the methanol stoichiometry high enough to avoid depleting methanol at the anode catalyst layer and incurring a transition to first-order methanol kinetics [26]. Substituting Eqs. (12) and (13) into Eq. (11) results in the following expression for the cell potential:

$$V_{cell} = U^{\theta} - i\frac{\kappa_{mem}}{L_{mem}} - i\frac{2L_{cl}}{\kappa_{cl}} - \frac{RT}{F\alpha_a}\ln\left(\frac{i}{i_a^0}\right) + \frac{RT}{F\alpha_c}\ln\left(\eta\frac{P_{O_2,c}}{P_{O_2,ref}}\frac{i_c^0}{i+i_x}\right). \tag{14}$$

It is clear that we must use a numerical method to solve for the current in Eq. (14). However, in order to find the desired current, we must first find an expression for the crossover current i_x in terms of the desired current i and other known variables.

2.3.2. Determination of crossover current and total current

To write i_x in terms of i we refer to our previous work [11] concerning the methanol concentration in the anode backing layer and in the membrane. The crossover current is described in terms of the feed concentration c_{feed} and the concentration at the anode catalyst layer c_{anode} as follows:

$$i_x = 6F\left(\frac{D^{eff}_{MeOH-H_2O}}{L_{back,a}}\right)\left(c_{feed} - c_{anode}\right) - i. \tag{15}$$

The crossover current can also be described using the dimensionless parameter ν.

$$i_x = \left(i_{lim,a} - i\right)\left(\frac{\nu}{1+\nu}\right). \tag{16}$$

Substituting Eq. (15) into Eq. (16) and solving for c_{anode} produces a relationship between c_{anode} and c_{feed}

$$c_{anode} = \left(1 - \frac{i}{i_{lim,a}}\right)\left(\frac{1}{1+\nu}\right)c_{feed}. \tag{17}$$

Further substitution of $i_{lim,a} = 6F(D^{eff}_{MeOH-H_2O}/L_{back,a})c_{feed}$ results the following expression for c_{anode}:

$$c_{anode} = \frac{\psi c_{feed} - c^0_{feed}}{\psi(1+\nu)}. \tag{18}$$

Eq. (18) shows that c_{anode} is dependent on c_{feed} at the corresponding location in the flow channel, the initial feed concentration c^0_{feed}, the dimensionless ratio ν, and $\psi = i^0_{lim,a}/i$, which is the limiting current at the anode entrance normalized by the desired current.

Removing ψ from the denominator and substituting the above expression for c_{anode} into Eq. (15) results in

$$i_x = \frac{i_{lim,a}}{c_{feed}}\frac{i}{i^0_{lim,a}}\left(\frac{\psi\nu c_{feed} + c^0_{feed}}{(1+\nu)}\right) - i. \tag{19}$$

Noting that $i_{lim,a}/i^0_{lim,a} = c_{feed}/c^0_{feed}$, we arrive at the desired relation for i_x in terms of i.

$$i_x = i\left(\frac{\psi\nu c_{feed} + c^o_{feed}}{c^o_{feed}(1+\nu)} - 1\right). \tag{20}$$

Now we are prepared to make the appropriate substitutions and solve Eq. (14) for i. The solution is performed in MATLAB using the root-finding function *fzero* along each cross-section of the cell. To obtain an average cell current the sum of the cross-sectional currents is divided by the number of steps.

2.4. Consumption of methanol and oxygen in the flow channels

2.4.1. Anode flow channel

Having the ability to find the local current density as a function of the local methanol concentration and oxygen pressure in the flow channels, we now must determine the consumption of methanol and oxygen in the flow channels as we move from one step to the next (Fig. 2).

Assuming the velocity v_{MeOH} of methanol in the flow channel is constant, the total flow rate of methanol in the anode flow channel is given by

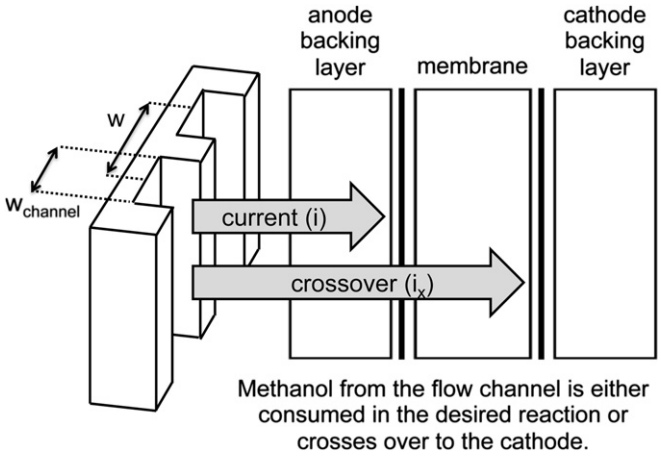

Fig. 2. Methanol consumption in the fuel cell.

$$N_{\mathrm{MeOH}}^{\mathrm{chan}} = c_{\mathrm{feed}} A_{\mathrm{chan}} v_{\mathrm{MeOH}}. \quad (21)$$

where $A_{\mathrm{chan}} = w_{\mathrm{chan}} h_{\mathrm{chan}}$. The change in feed concentration between each step as we move down the flow channel is

$$\frac{\partial c_{\mathrm{feed}}}{\partial z'} = -N_{\mathrm{MeOH}}^{\mathrm{back}} \left(\frac{w_{\mathrm{sep}} L_{\mathrm{chan}}}{A_{\mathrm{chan}} v_{\mathrm{MeOH}}}\right) = -\left(\frac{i+i_x}{6F}\right)\left(\frac{w_{\mathrm{sep}} L_{\mathrm{chan}}}{A_{\mathrm{chan}} v_{\mathrm{MeOH}}}\right). \quad (22)$$

where $z' = z/L_{\mathrm{chan}}$ is the normalized distance down the channel, and w_{sep} is the channel separation width, that is, the width of electrode perpendicular to the channel flow that is fed by a single channel. $w_{\mathrm{sep}} L_{\mathrm{chan}}$ is the area of the anode that receives the methanol flowing through the channel. The effects of other parallel channels are ignored.

Noting the presence of the crossover current term i_x, we substitute Eq. (20) to obtain

$$\frac{\partial c_{\mathrm{feed}}}{\partial z'} = -\left(\frac{i}{6F}\right)\left(\frac{\psi \nu c_{\mathrm{feed}} - c_{\mathrm{feed}}^0}{c_{\mathrm{feed}}^0 (1+\nu)}\right)\left(\frac{w_{\mathrm{sep}} L_{\mathrm{chan}}}{A_{\mathrm{chan}} \nu}\right). \quad (23)$$

We can now define the stoichiometric ratio for the methanol flow as

$$s_{\mathrm{MeOH}} = \frac{c_{\mathrm{feed}}^0}{i/6F} \frac{A_{\mathrm{chan}} \nu}{L_{\mathrm{chan}} w_{\mathrm{sep}}} \quad (24)$$

and derive an expression for the change in the feed concentration

$$\frac{\partial c_{\mathrm{feed}}}{\partial z'} = -\left(\frac{1}{s_{\mathrm{MeOH}}}\right)\left(\frac{\psi \nu c_{\mathrm{feed}} - c_{\mathrm{feed}}^0}{(1+\nu)}\right). \quad (25)$$

The stoichiometric ratio is the rate at which methanol is delivered to the inlet of the cell relative to the amount of methanol that is consumed in the preferred electrochemical reaction. Hence, it represents the inverse of fuel utilization or fuel efficiency. In order to discretize the flow channel and apply the one-dimensional model from Sections 2.1 to 2.3, we apply a first-order forward difference, $f(x+h) = f(x) + hf'x$, where $h = L_{\mathrm{chan}}/n$ is the step size and n is the total number of steps. Then we create the following expression for c_{feed} at step $k+1$ based on c_{feed} and the current i at step k.

$$c_{\mathrm{feed}}(k+1) = c_{\mathrm{feed}}(k) - \left(\frac{1}{\mathrm{siz}}\right)\left(\frac{1}{s_{\mathrm{MeOH}}}\right)\left(\frac{\psi \nu c_{\mathrm{feed}} - c_{\mathrm{feed}}^0}{(1+\nu)}\right). \quad (26)$$

2.4.2. Cathode flow channel

In the cathode flow channel, where the oxygen reactant is a gas, we must consider the pressure drop of the air stream in addition to the consumption of oxygen. We cannot assume that the velocity of the air stream is constant as we do for the velocity of the liquid methanol/water solution in the anode flow channel. We do assume that the absolute pressure of water vapor remains constant throughout the flow channel. If the inlet flow is dry, then the water vapor pressure is set to zero, and if it is humidified, then the water vapor pressure is assumed to be its saturated value given in Eq. (1). This simplification is necessary given that changes in water content are not treated in the backing layer, but it can lead to significant error at high current when the water generation is high. Because of these assumptions, the pressure drop only affects the nitrogen and oxygen pressures. In general terms, according to Darcy's Law, the pressure drop is

$$\frac{\partial P_{\mathrm{air},f}}{\partial z} = -\frac{\mu_{\mathrm{air}}}{K} v_{\mathrm{air},f} = -\frac{\mu_{\mathrm{air}}}{K} \frac{N_{\mathrm{air},f}}{A_{\mathrm{chan}}} \frac{RT}{P_{\mathrm{air},f}}. \quad (27)$$

where $K = D_h^2/2f\mathrm{Re}$ represents the cross-sectional area to flow. Re is the Reynolds number, f is a friction factor, and their product is equal to 14.2296 for a square channel [23]. D_h is the hydraulic diameter and is equal to four times the area of the channel divided by the perimeter. μ_{air} is the dynamic viscosity of the air mixture and is a function of the mole fraction of all three components in the mixture

$$\mu_{\mathrm{air}} = \sum_{i=1}^{N} \frac{y_i \mu_i}{\sum_{j=1}^{N} y_i \Phi_i}. \quad (28)$$

where N is the total number of species in the mixture, y_i and y_j are the mole fractions of species i and j, and Φ_i is a sum of dimensionless ratios. For an in depth analysis of the derivation of μ_{air}, we refer the reader to pp. 153–155 in Ref. [23]. At 65 °C, μ_{air} is about 1.6×10^{-5} Pa s^{-1}, depending on the values of the mole fractions.

Substituting for k and noting that $N_{\mathrm{air},f}/P_{\mathrm{air},f} = N_{\mathrm{O_2},f}/P_{\mathrm{O_2},f}$, we obtain a final expression for the pressure drop as a function of the oxygen flow rate, oxygen pressure, and known parameters

$$\frac{\partial P_{\mathrm{air},f}}{\partial z} = -\frac{2f\mathrm{Re}\mu_{\mathrm{air}}}{D_h^2} \frac{N_{\mathrm{O_2},f}}{A_{\mathrm{chan}}} \frac{RT}{P_{\mathrm{O_2},f}}. \quad (29)$$

Using a forward difference to discretize this equation, as we did with Eq. (25), results in

$$P_{\mathrm{air},f}(k+1) = P_{\mathrm{air},f}(k) - \left(\frac{L_{\mathrm{chan}}}{\mathrm{siz}}\right)\left(\frac{2f\mathrm{Re}\mu_{\mathrm{air}}(k)}{D_h^2}\right)\left(\frac{N_{\mathrm{O_2},f}(k)}{A_{\mathrm{chan}}} \frac{RT}{P_{\mathrm{O_2},f}(k)}\right). \quad (30)$$

Therefore the pressure drop at step $k+1$ is determined by the ratio of the oxygen flow rate to the oxygen pressure at step k. The change in oxygen flow rate is simply a function of the total current, and that expression can be discretized to solve for $N_{\mathrm{O_2},f}(k)$.

$$N_{\mathrm{O_2},f}(k+1) = N_{\mathrm{O_2},f}(k) - \frac{i+i_x}{4F}\left(\frac{w_{\mathrm{sep}} L_{\mathrm{chan}}}{\mathrm{siz}}\right). \quad (31)$$

Determining the local oxygen pressure $P_{\mathrm{O_2},f}(k)$ is a bit more challenging. The expression for the consumption of oxygen in the cathode flow channel is derived in a similar manner as for methanol in the anode. The change in oxygen pressure due to consumption is

$$\frac{\partial P_{\mathrm{O_2},f}}{\partial z} = -N_{\mathrm{O_2}}^{\mathrm{back}}\left(\frac{w_{\mathrm{sep}} RT}{A_{\mathrm{chan}} v_{\mathrm{O_2},f}}\right) = -\left(\frac{i+i_x}{4F}\right)\left(\frac{P_{\mathrm{O_2},f}}{N_{\mathrm{O_2},f}}\right) w_{\mathrm{sep}}. \quad (32)$$

where the substitution $v_{\mathrm{O_2},f} = v_{\mathrm{air},f} = (N_{\mathrm{O_2},f}/A_{\mathrm{chan}})(RT/P_{\mathrm{O_2},f})$ is made. Substituting Eq. (20) for i_x, we find an expression for the change in oxygen pressure that is similar to Eq. (23)

$$\frac{\partial P_{\mathrm{O_2},f}}{\partial z} = -\left(\frac{i}{4F}\right)\left(\frac{\psi \nu c_{\mathrm{feed}} - c_{\mathrm{feed}}^0}{c_{\mathrm{feed}}^0 (1+\nu)}\right)\left(\frac{P_{\mathrm{O_2},f}}{N_{\mathrm{O_2},f}}\right) w_{\mathrm{sep}}. \quad (33)$$

Discretizing Eq. (33) and adding it to Eq. (30) results in an expression for the change in the total pressure of the air inlet stream at each step

$$P_{\mathrm{air},f}(k+1) = P_{\mathrm{air},f}(k) - \left(\frac{w_{\mathrm{sep}} L_{\mathrm{chan}}}{\mathrm{siz}}\right)\left(\frac{i}{4F}\right)\left(\frac{\psi \nu c_{\mathrm{feed}}(k) - c_{\mathrm{feed}}^0}{c_{\mathrm{feed}}^0 (1+\nu)}\right) \times \left(\frac{P_{\mathrm{O_2},f}(k)}{N_{\mathrm{O_2},f}(k)}\right) - \left(\frac{L_{\mathrm{chan}}}{\mathrm{siz}}\right)\left(\frac{2f\mathrm{Re}\mu_{\mathrm{air}}(k)}{D_h^2}\right) \times \left(\frac{N_{\mathrm{O_2},f}(k)}{A_{\mathrm{chan}}} \frac{RT}{P_{\mathrm{O_2},f}(k)}\right). \quad (34)$$

Because the total pressure is the sum of the partial pressures, with the water vapor pressure being constant, we can relate the nitrogen and oxygen pressures in order to make substitutions and solve for each partial pressure individually: $P_{O_2,f} = P_{N_2,f}(N_{O_2,f}/N_{N_2,f})$ and $P_{N_2,f} = P_{O_2,f}(N_{N_2,f}/N_{O_2,f})$. The analysis above applies to a system where the flow channels are in a coflow configuration, in which the methanol and oxygen flow in the same direction through the fuel cell. If we desire, we can add the change in oxygen pressure between steps instead of subtracting it and thereby simulate a counterflow configuration, in which the methanol and oxygen flow in opposite directions. The only difficulty in that situation is the need to define the oxygen pressure at the channel outlet and the oxygen flow rate at the inlet, both of which change as we move down the flow channel. For the sake of simplicity, we choose to use a coflow configuration in the analysis below. The oxygen stoichiometric ratio remains very high (always above 10) in the experimental data used for validating the model, which justifies this approach. Furthermore, the flow channels have a single-serpentine design, and there is probably a large amount of under-rib transport. At the high flow rates we are considering, we expect there to be little difference between coflow and counterflow in the current/potential regimes that are not mass-transfer limited.

3. Experimental validation

3.1. Nafion membranes with optimized catalyst layers

The purpose of this model is to quickly and easily determine the effect of materials properties and operational parameters, especially the membrane permeability, conductivity, and thickness and the methanol and oxygen flow rates, on the performance and the required size of the DMFC system. In order to fit certain parameters and accurately predict the performance of real systems, we need to validate the model with a control set of experimental data. One drawback to this model is the assumption of a negligibly thin catalyst layer and simple zero-order (methanol) or first-order (oxygen) Tafel kinetics for the complex reactions taking place at the anode and cathode catalyst layers. Hence, the anodic and cathodic exchange current densities (i_a^0 and i_c^0) and the symmetry coefficients (α_a and α_c) must be adjusted to fit experimental data. After comparison with the data, we found that the addition of a contact resistance term R_c was unnecessary. The base values that we use for all of the physical properties are listed in Table 1 and do not change in the following sections unless otherwise noted. The values of all the kinetic and resistive properties are listed in Table 2. It is important to note that we assume liquid water to be almost as effective as a solid medium at preventing gas diffusion. Therefore, we account for the effect of liquid water in the cathode by lowering the porosity of the cathode considerably relative to the anode.

As an initial check, we used a base case scenario (Nafion 115, 250 sccm oxygen flow rate, and 2 ml min^{-1} methanol flow rate) and varied the temperature (65 °C or 90 °C) and the cathode flow composition (air or pure oxygen). The experiments were performed with a 1 M MeOH feed at the anode and 20 psi of backpressure at the cathode. The resulting four cases for a single cell with a 5 cm^2 MEA are shown in Fig. 1 below. The MEAs were fabricated by spraying the respective catalyst layer inks onto each side of the Nafion membrane and then hot-pressing the carbon cloth backing layers onto each side. The catalyst loading was 2.5 mg cm^{-2} Pt/Ru on the anode and 2.5 mg cm^{-2} Pt on the cathode on unsupported carbon black. This validation was performed to determine the accuracy of the temperature-dependent diffusion coefficients, conductivities, and exchange current densities as well as to verify our assumption of a constant water vapor pressure in the cathode. These experiments also tested the validity of our choice to incorporate the effects of liquid water and carbon dioxide into an effective diffusion coefficient rather than consider those components explicitly.

Table 1
Physical properties for experimental validation.

Parameter (unit)	Value	Reference
$D_{O_2-H_2O}$ (cm^2 s^{-1})	$6.436 \times 10^{-6} * T^{1.823}/p$(in atm)	O'Hayre et al. [23]
$D_{O_2-N_2}$ (cm^2 s^{-1})	$4.2 \times 10^{-7} * T^{2.334}/p$(in atm)	O'Hayre et al. [23]
D_{MeOH-H_2O} (cm^2 s^{-1})	$10^{-1.416 - 999.778/T}$	Yaws [30]
D_{mem} (cm^2 s^{-1})	$4.9 \times 10^{-6} * e^{2416(1/333 - 1/T)}$	Kauranen and Skou [31]
ε_a (dimensionless)	0.7	Wang and Wang [20]
ε_c (dimensionless)	0.35	Fitted to data
ε_{cl} (dimensionless)	0.1	Assumed
ϕ_{Nafion} (dimensionless)	0.058	Measured
$L_{back,a} = L_{back,c}$ (cm)	0.02	Assumed
L_{mem} (cm)	0.0128	Assumed
ρ_{H_2O} (g cm^{-3})	$1.1603 - 5.371 \times 10^{-4} * T$	Incropera et al. [21]
ξ_{H_2O} (dimensionless)	2.5	Zawodzinski et al. [32]
ξ'_{MeOH} (dimensionless)	$\xi_{H_2O} * 18/\rho_{H_2O}$	Calculated
w_{sep} (cm)	0.2	Measured
L_{chan} (cm)	25	Measured
A_{chan} (cm^2)	0.01	Measured

The primary discrepancy between the model and the experiments exists in the mass-transport region, especially in the 65 °C case with air. We believe this discrepancy exists mostly because our model does not allow for varying water content in the catalyst layer, gas diffusion layer, and flow channel of the cathode. High current density generally corresponds with high water crossover and generation rates and lower effective oxygen diffusion coefficients, which decreases performance. However, accounting for these variations would have eliminated our ability to derive analytic expressions for the gas concentrations across the thickness of the cell. We decided that a modeling scheme which can match the experimental performance over the current and potential ranges of interest (generally less than 300 mA cm^{-2}) with a simple set of assumptions and a fast run time (usually less than 1 min) is of greater interest to the engineering problems of system sizing and stack optimization.

Experimental results, including the results shown in Fig. 3, often use deliberately high flow rates in order to maximize performance. However, in a real system, it might behoove the designer to take a small cut in performance by lowering the flow rate to say, 50 sccm, such that the air blower and the compressor consume less power. The ability of this model to accurately predict fuel cell performance for a variety of methanol and oxygen flow rates will be important when we consider optimizing the size of system components in Section 4.

3.2. Low-crossover crosslinked blend membranes

The cases above all employ Nafion membranes, but much work has been done in recent years to develop new membranes with lower methanol crossover than Nafion and comparable proton conductivity and mechanical properties. In particular, Zhu et al. have reported novel crosslinked membranes based on a blend of

Table 2
Kinetic and resistive properties for Nafion membranes.

Parameter (unit)	Value	Reference
i_a^0 (A cm^{-2})	3.5×10^{-5}	Fitted to data
i_c^0 (A cm^{-2})	3.0×10^{-7}	Fitted to data
α_a (dimensionless)	0.8	Fitted to data
α_c (dimensionless)	0.875	Fitted to data
κ_{mem} (S cm^{-1})	$0.111 * e^{1268(1/303 - 1/T)}$	O'Hayre et al. [23]
κ_{cla} (S cm^{-1})	$0.001 * e^{1268(1/298 - 1/T)}$	Havranek and Wippermann [33]
κ_{clc} (S cm^{-1})	$0.0026 * e^{1268(1/298 - 1/T)}$	Saab et al. [34]

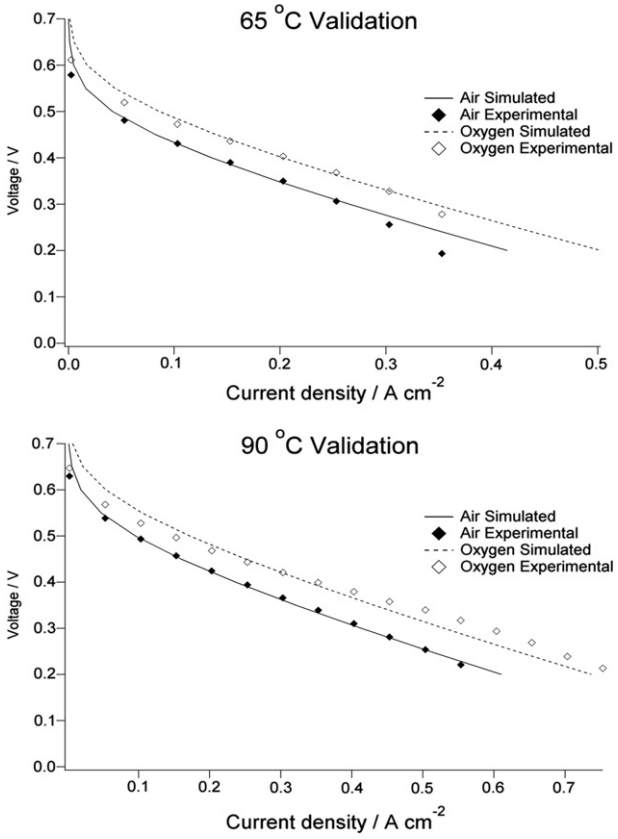

Fig. 3. Comparison of simulations to experimental data at 65 °C and 90 °C. The base case scenario presented here uses a Nafion 115 membrane, 250 sccm oxygen flow rate with 20 psi of backpressure, and 2 ml min^{-1} methanol flow rate with 1 M methanol feed concentration.

sulfonated poly(ether ether ketone) and carboxylated polysulfone that showed a dramatic improvement in performance compared to Nafion [27]. They kindly made that data available in tabular form along with physical property data for our use in Figs. 4 and 5. This section describes a case study in which we compared our model with the data for their C-10 membrane. These tests were run at 65 °C and 1 M MeOH using a humidified oxygen feed at a 200 sccm

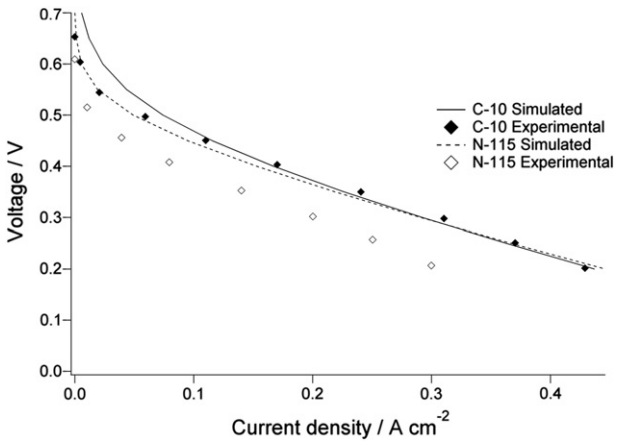

Fig. 4. Comparison of experiments and simulations for the C-10 blend membrane and Nafion 115 membrane at 65 °C. This scenario uses a 2.5 ml min^{-1} methanol flow rate with 1 M methanol feed concentration, and a 200 sccm oxygen flow rate with a humidified pure oxygen feed and no backpressure. Experimental data is from Zhu et al. [13].

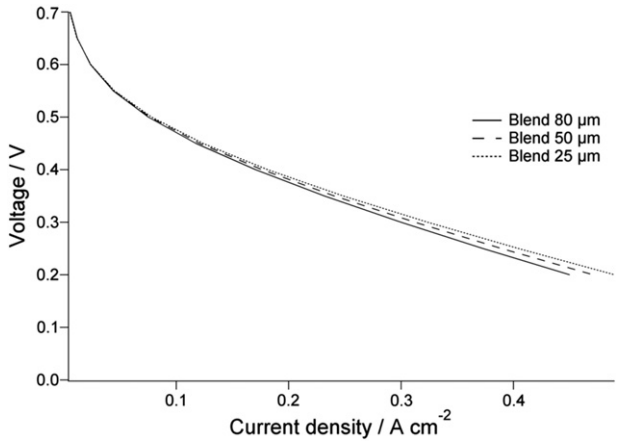

Fig. 5. Performance of the C-10 blend membrane as a function of membrane thickness. The parameters and operating conditions are identical to what is used for the low-crossover membrane in Fig. 4.

flow rate. The MEAs in this case used a different catalyst loading than in the previous case (2.0 mg cm^{-2} vs. 2.5 mg cm^{-2} above) and were fabricated by painting the catalyst inks onto the carbon cloth backing layers and then hot-pressing each of the two sets onto opposite sides of the Nafion membrane. Therefore, we had to adjust the exchange current densities and symmetry coefficients to account for the differences in the catalyst layers. The new kinetic parameters, as well as the new membrane properties, are given in Table 3.

Fig. 4 above compares Nafion 115 to the new membranes with our simulation overlapping both data sets. Our model predicts a noticeable improvement when using the new membranes, but not as a large an improvement as the experiments show. Indeed, the experimental results at high current are surprising because in that region we would expect the higher ohmic resistance in the blend membranes to counteract performance gains from lower methanol crossover. There are several experiments in the literature, most notably from Ge and Liu [28], running under similar conditions that show much better performance from Nafion membranes than what is shown in Fig. 4. We believe the discrepancy at higher currents is due to mass-transport problems in the experiment, specifically water management, for which our model does not account. Also, a different construction of the catalyst layers, as was done with the experiments shown in Fig. 3, might lead to better performance for both the Nafion and the blend membranes. Finally, the discrepancies at low current could be the result of the methanol diffusion coefficient in the blend membranes being higher during the experiment than what was measured prior to the experiment.

One advantage of the blend membranes is that they can be made thinner without significantly increasing the methanol crossover, which can more than compensate for the decrease in specific conductivity when compared to Nafion. Fig. 5 simulates the performance of the C-10 membrane reported by Zhu et al. [27] for

Table 3
Kinetic and membrane properties for blend membranes.

Parameter (unit)	Value	Reference
i_a^0 (cm^{-2} s^{-1})	3.0×10^{-5}	Fitted to data
i_c^0 (cm^{-2} s^{-1})	2.0×10^{-7}	Fitted to data
α_a (dimensionless)	0.875	Fitted to data
α_c (dimensionless)	0.925	Fitted to data
κ_{mem} (S cm^{-1})	0.107	Zhu et al.
L_{mem} (cm)	0.01	Zhu et al.
D_{mem} (cm^2 s^{-1})	1.0×10^{-8}	Measured

a variety of thicknesses under the conditions given in Section 3. Fig. 6 does the same with Nafion membranes. While the thinner Nafion membranes suffer from noticeable performance declines at low current due to crossover, the blend membranes show no drop in performance. As we mentioned above, the measured methanol diffusion coefficient might be lower than the actual value, but the model still clearly shows that the blend membranes should be made as thin as manufacturing tolerances allow. The reduction in ohmic resistance more than compensates for the small increase in methanol crossover.

Aside from improved performance, the lower methanol crossover rates of the new membranes results in improved fuel efficiency. If we want to calculate the maximum fuel efficiency of the fuel cell we can perform an iterative reduction of the methanol stoichiometric ratio until the methanol concentration at the anode reaches the first-order transition value. Also of importance when it comes to optimizing the DMFC system with new membranes are the properties of the backing layers. The thickness and porosity of the backing layers must strike a balance between allowing reactants to diffuse to the catalyst layers and providing an effective barrier, both physically and chemically, between the reaction zones and the flow channels. The anode backing layer is of particular importance because it must allow enough methanol to reach the anode catalyst layer so as to promote the desired reaction while not allowing so much methanol so as to promote crossover. Our previous work [4] addresses in detail the issues of fuel efficiency and backing layer properties, so in order to avoid repetition, this paper will not discuss these issues at length.

4. The effect of methanol and oxygen flow rates on system size and performance

Because portability is of primary importance in many applications where DMFCs might be used, we want to use this model to compare the power consumption of the air blower and compressor to the stack power output for a range of methanol and air flow rates. The less methanol and oxygen that are used and the more slowly those reactants are passed through the flow channels, the smaller we can make the supporting system components. Ideally, there would be no methanol crossover, and all of the reactants in the system would either be consumed in the desired reaction or exit the flow channels, perhaps being recirculated through the system to be consumed later. In this case, the size of the supporting system components would be solely dependent on the demand for current. However, the existence of crossover and the potential for wasted fuel means that the size of the tank and the blower also depends on the fuel efficiency.

If reducing the size of the system components were our only concern, then we would like to run the cell as lean as possible with a very low stoichiometric ratio. However, running a lean feed will result in performance losses compared to running at a high stoichiometric ratio. We are especially concerned with avoiding the transition from zero-order to first-order kinetics for the methanol oxidation reaction. Rather than model this complicated transition, which would require a substantial increase in overpotential at the anode and a corresponding loss in performance [26], we ensure that the optimized system remains above any such transition by requiring the feed concentration to remain above a minimum value throughout the flow channel. In doing so, we impose a constraint on the minimum allowable stoichiometric ratio at the anode. At the cathode, our only constraint on the stoichiometric ratio is that it remains above unity.

It is important to note that the analysis in this section does not constitute an optimization study in the true spirit of the term. We iterate through a defined set of flow rates for a few specific scenarios instead of using an optimization function to explore the entire parameter space. A more thorough optimization analysis could be done with this model, but we choose not to do so here for the sake of brevity. Hence, the more accurate term to describe what is done here is a sensitivity analysis. The goal of this section is to illustrate how the model can be applied across a wide range of a given parameter space and how it can provide guidelines for certain parameters.

For a single fuel cell, the size of the fuel tank $V_{\tan k}$ scales linearly with the flow rate at the anode inlet $N_{\mathrm{MeOH}}^{\mathrm{input}}$, the time of operation t and the molar volume of the methanol and water feed stream $\overline{V}_{\mathrm{feed}}$: $V_{\tan k} = N_{\mathrm{MeOH}}^{\mathrm{input}} \overline{V}_{\mathrm{feed}} t$, where $N_{\mathrm{MeOH}}^{\mathrm{input}} = c_{\mathrm{feed}}^{0} A_{\mathrm{chan}} \nu_{\mathrm{MeOH}}$ as in Eq. (21). We have already seen in Fig. 6 how the performance of the fuel cell is largely independent of the anode flow rate due to zero-order kinetics, so in that sense, we want to run at as low a flow rate as possible to avoid crossover and wasted fuel. However, there must be a point at which the flow rate is not high enough to sustain zero-order kinetics. Using the model to predict this minimum flow rate would be useful in determining parameters for fuel cell design and operation.

The scenario presented in Fig. 7 above compares the power output of a fuel cell operating at 300 mA cm^{-2} current using Nafion 115 to fuel cells using blend membranes of the same thicknesses (represented by the blue lines) as in Fig. 5. The operating conditions

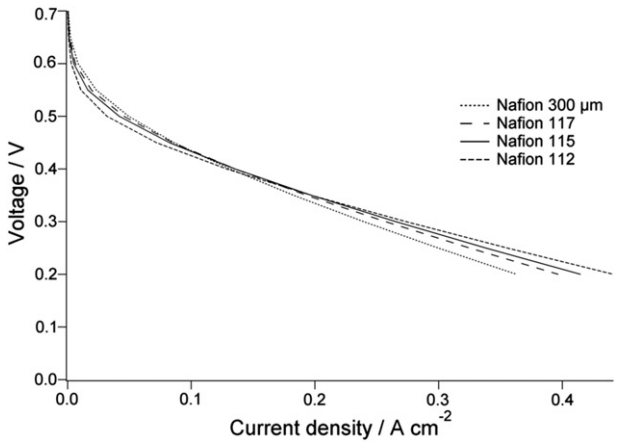

Fig. 6. Performance of the Nafion membranes as a function of membrane thickness. The parameters and operating conditions are identical to what is used for the Nafion 115 membrane in Fig. 3.

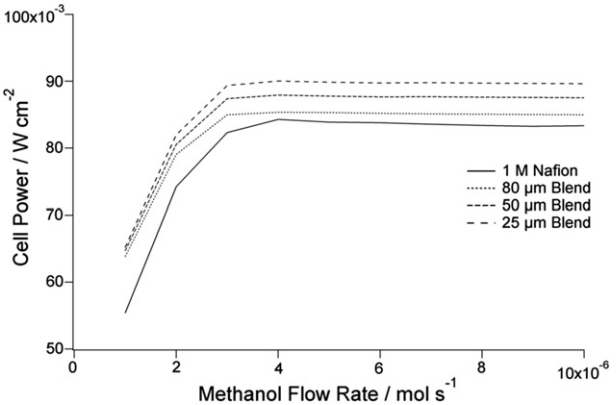

Fig. 7. Cell output power as a function of methanol flow rate for a desired current of 0.3 A cm^{-2} using Nafion 115 and C-10 blend membranes. All other parameters and operating conditions are identical to what is used in Fig. 3.

and the cell design are the same for the Nafion and blend membranes. The blend membranes are very effective at preventing methanol crossover, so the model tells us that we should manufacture them as thin as possible in order to lower the ohmic resistance, especially at high current. Of course, the limits of the manufacturing process and the desire to maintain good mechanical properties and durability will limit our ability to reduce the membrane thickness.

In this case, the minimum methanol flow rate is 4×10^{-6} mol s^{-1}, which corresponds to 0.25 ml min^{-1} and an average methanol stoichiometric ratio of 1.6. Since the model cannot handle the transition to first-order kinetics, the three points below that transition are generated by lowering the desired current until the methanol concentration remains above the transition value all the way to the anode exit. Hence, the power output of the cell must decrease either by incurring a drop in cell voltage due to the transition to first-order kinetics or by lowering the current until that transition is avoided. In designing a system under our given conditions, we would want to keep the methanol flow rate close to this value but safely above it to maximize performance and efficiency.

The situation is similar when we consider the oxygen flow rate under the same set of conditions. Given the low flow rates that we are using, the power consumption of the air blower and air compressor will scale linearly with the flow rate in the cathode flow channel. Therefore, as with the anode flow rate, we would expect at to see a point at which the extra power generated by the fuel cell does not justify increasing the flow rate. The power output of the compressor is given by [7]

$$\text{Power}_{\text{comp}} = \left[\frac{371TN_{O_2}^{\text{input}}\gamma}{(\gamma-1)E_{\text{comp}}}\right]\left[\left(\frac{P_{O_2,f}^{0}}{P_{O_2,\text{ref}}}\right)^{(1-(1/\gamma))} - 1\right]. \quad (35)$$

where γ is the heat capacity at constant pressure divided by that at constant volume ($\gamma = 1.4$), $P_{O_2,f}^{0}$ is the inlet oxygen pressure in the cathode flow channel, E_{comp} is the air compressor efficiency (assumed to be 0.8) and the coefficient of 371 has units of J K^{-1} m^{-3}.

The blower power output can be found using the specific fan power (SFP) as follows:

$$\text{Power}_{\text{blower}} = \text{SFP}{*}N_{O_2}^{\text{input}}. \quad (36)$$

The lowest SFP values for small commercial fans operating under normal conditions is approximately 500 W s m^{-3} [29], so we choose to use that value through this analysis. Note the need to convert the oxygen flow rate from mol s^{-1} to m^3 s^{-1} through multiplication by the molar volume. Although the compressor uses much more power than the blower, the performance gain achieved by raising the cathode input pressure is substantial and the need to maintain a high oxygen concentration in the presence of methanol crossover is imperative. Therefore, we chose to include a compressor throughout this analysis. Subtracting these parasitic losses from the power output of the fuel cells provides us with an expression for the net power output of the system

$$\text{Power}_{\text{system}} = V_{\text{cell}}I_{\text{cell}}(\#\text{cells}) - \text{Power}_{\text{comp}} - \text{Power}_{\text{blower}} - \text{Power}_{\text{pump}}. \quad (37)$$

Because the analysis below is only concerned with the oxygen flow rate, the parasitic losses from the methanol pump $\text{Power}_{\text{pump}}$ are ignored in the calculation of the system power output.

Fig. 8 above shows the power output of a DMFC stack containing 100 5 cm^2 cells as a function of oxygen flow rate. As expected, the

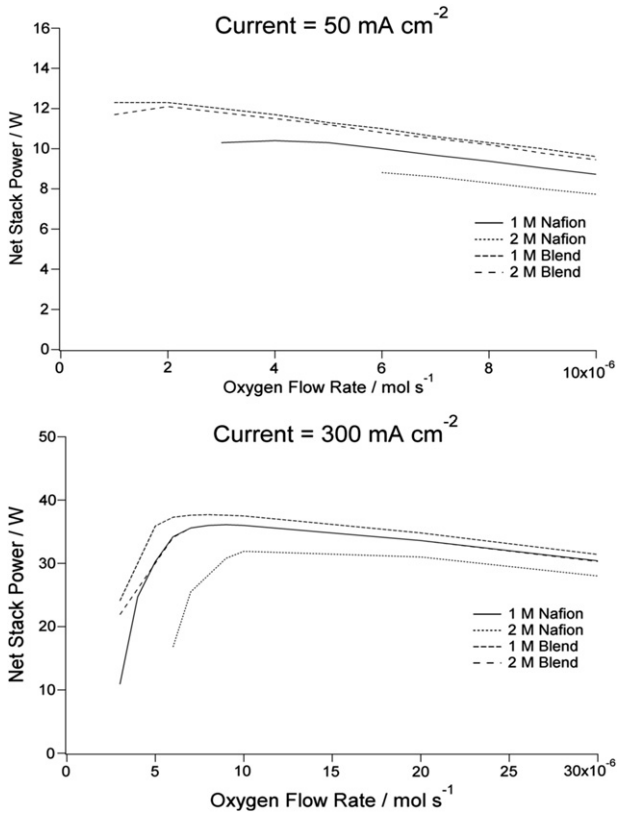

Fig. 8. Net power output of a 100 cell stack as a function of oxygen flow rate with 0.05 and 0.3 A cm^{-2} currents using Nafion 115 and C-10 blend membranes. All other parameters and operating conditions are identical to what is used in Fig. 3.

80 μm thick blend membranes outperform the Nafion 115 membranes, and the 1 M MeOH feed stream is always better for performance than 2 M MeOH due to zero-order methanol kinetics. Similar to what was done in Fig. 7, the desired current is lowered at low flow rates in order to keep the oxygen pressure above zero across the entire cathode. However, in some cases at 50 mA cm^{-2} the current cannot be lowered any further, and so the fuel cell cannot run at all below those cutoff flow rates. The 2 M Nafion 115 case in particular shows a much higher cutoff flow rate than the blend membranes. This low current scenario is where the blend membranes have the greatest advantage over the Nafion membranes.

In all of these cases, the power demand of the compressor and the blower is a substantial fraction of the power output of the fuel cell stack. At the optimum flow rate in the 300 mA cm^{-2} scenario, the power output of the 100 cell stack is about 40 W, and the power consumption of the compressor and the blower is about 4 W, or 10% of the total power output. That fraction only gets larger as the flow rate increases because the performance gains become smaller and smaller while the power consumption of the system components continues to increase linearly. The oxygen reduction reaction is first-order, so there is a noticeable performance penalty to be paid for operating close to the cutoff flow rate. However, until the flow rate is within about 2×10^{-6} mol s^{-1} of the cutoff flow rate, that penalty is more than compensated for by the lower power consumption of the system components. Therefore, as with the methanol flow rate, it is important to keep the oxygen flow rate as low as possible while not allowing the oxygen pressure to fall close to zero such that substantial performance losses are incurred.

5. Conclusion

In this work, a simple engineering model is developed that directly relates the materials properties of the direct methanol fuel cell – including diffusion coefficients, membrane thickness, and proton conductivity – and operating parameters – most notably the methanol and oxygen flow rates – to the stack performance and the size of system components such as the methanol storage tank and the air blower. The model is created by deriving analytic solutions for the methanol and oxygen concentrations across the thickness of the fuel cell and by applying Tafel kinetics to determine the average cell current density for a fixed cell voltage. The benefits of the model include a run time of less than a minute for a single current–voltage curve in a MATLAB simulation environment and the ability to handle a wide range of parameter spaces.

The model was validated using experimental current–voltage data taken at 65 °C and 90 °C with air oxygen cathode feeds. It was then applied to forecast the benefits of using new low-crossover membranes and was compared to published data from Zhu et al. Finally, the model was used in a case study to illustrate the effect of changing the methanol and oxygen flow rates on fuel cell performance and the net power output of the fuel cell stack. The tradeoff that exists between stack performance, the methanol storage tank, and the power consumption of the air blower, air compressor, and other components dictates that there exists an optimum set of operating conditions for any portable DMFC with size constraints.

Acknowledgments

Financial support by the Office of Naval Research MURI grant No. N00014-07-1-0758 is gratefully acknowledged.

Glossary

Roman Symbols

A	superficial area of the anode, cm^2
A_{chan}	cross-sectional area of the flow channel, cm^2
c_{anode}	methanol concentration at the anode catalyst layer, mol cm^{-3}
c_{feed}	methanol concentration in the anode feed stream, mol cm^{-3}
c^0_{feed}	methanol feed concentration at channel inlet ($z = 0$), mol cm^{-3}
c_{H_2O}	concentration of liquid water in the membrane, mol cm^{-3}
D_{i-j}	diffusion coefficient of component i in component, $cm^2\ s^{-1}$
D^{eff}_{i-j}	effective diffusion coefficient of component i in component j, $cm^2\ s^{-1}$
D_{mem}	diffusion coefficient of methanol in the membrane, $cm^2\ s^{-1}$
$D_{O_2,cl}$	D^{eff} of oxygen in the cathode catalyst layer, $cm^2\ s^{-1}$
d_h	hydraulic diameter of the flow channel, cm
E_{comp}	air compressor efficiency, dimensionless
f	friction coefficient of air in the flow channel, dimensionless
h	size of each iteration step in the flow channels, cm
i	current through the external circuit, A cm^{-2}
i_x	crossover current, A cm^{-2}
i^0_a	anodic reference exchange current density, A cm^{-2}
i^0_c	cathodic reference exchange current density, A cm^{-2}
$i_{lim,a}$	limiting current in the anode backing layer, A cm^{-2}
$i^0_{lim,a}$	backing layer limiting current at anode channel inlet, C $cm^{-2}\ s^{-1}$
k	cross-sectional area to flow in cathode flow channel, cm^2
$L_{back,a}$	thickness of the anode backing layer, cm
$L_{back,c}$	thickness of the cathode backing layer, cm
L_{mem}	thickness of the membrane, cm
L_{cl}	thickness of the catalyst layers, cm
L_{chan}	length of the flow channels, cm
n	total number of iterations down the flow channel, dimensionless
N^j_i	flow rate of component i through region j, mol s^{-1}
$N_{i,f}$	flow rate of component i in the cathode flow channel, mol s^{-1}
N^{input}_{MeOH}	methanol flow rate into the anode flow channel inlet, mol s^{-1}
$N^{input}_{O_2}$	oxygen flow rate into the cathode flow channel inlet, mol s^{-1}
P_i	absolute pressure of component i, N m^{-2}
$P_{i,f}$	pressure of component i in the bulk flow channel, N m^{-2}
$P_{O_2,s}$	oxygen pressure at the cathode backing layer surface, N m^{-2}
$P_{O_2,c}$	oxygen pressure at the cathode catalyst layer surface, N m^{-2}
$P_{O_2,ref}$	reference oxygen pressure, N m^{-2}
$P^0_{O_2,f}$	input oxygen pressure in the cathode flow channel, N m^{-2}
$P_{H_2O,sat}$	saturated vapor pressure of water, N m^{-2}
$P^{back}_{O_2}$	oxygen pressure in the cathode backing layer, N m^{-2}
$P^{conv}_{O_2}$	oxygen pressure in convective flow channel regions, N m^{-2}
P_{total}	total pressure in the cathode backing layer N m^{-2}
$Power_{comp}$	power consumed by the air compressor, W
$Power_{blower}$	power consumed by the air blower, W
Re	Reynolds number of cathode air flow, dimensionless
s_i	stoichiometric ratio of methanol or oxygen, dimensionless
Sh_F	Sherwood number for a square channel, dimensionless
SFP	specific fan power, W s m^{-3}
t	time of fuel cell operation, s
U^θ	standard cell potential, V
V_{anode}	anodic activation overpotential, V
$V_{cathode}$	cathodic activation overpotential, V
V_{cell}	total cell potential, V
$\overline{V}_{feed}$	molar volume of the methanol and water feed stream, $cm^3\ mol^{-1}$
v_{MeOH}	velocity of methanol in the anode flow channel, cm s^{-1}
$v_{air,f}$	velocity of air in the cathode flow channel, cm s^{-1}
$v_{O_2,f}$	velocity of oxygen in the cathode flow channel, cm s^{-1}
w_{sep}	flow channel separation width, cm
y_i	mole fraction of component i, dimensionless
z	distance down the flow channel, cm
z'	normalized distance down the flow channel, dimensionless

Greek Symbols

α_a	anodic transfer coefficient, dimensionless
α_c	cathodic transfer coefficient, dimensionless
ε_a	porosity of the anode backing layer, dimensionless
ε_c	porosity of the cathode backing layer, dimensionless
ε_{cl}	porosity of the catalyst layers, dimensionless
κ_{mem}	proton conductivity of the membrane, S cm^{-1}
κ_{cla}	proton conductivity of the anode catalyst layer, S cm^{-1}
κ_{clc}	proton conductivity of the cathode catalyst layer, S cm^{-1}
μ_i	dynamic viscosity of component i, Pa s^{-1}
η	effectiveness factor of cathode catalyst layer, dimensionless
ϕ_{Nafion}	Nafion volume fraction in the catalyst layer, dimensionless
Φ_i	sum of dimensionless ratios (see pp. 153–155 in Ref. [23]), dimensionless

ψ	ratio of i^0_{lim} to the current through the external circuit, dimensionless
ρ_{H_2O}	density of liquid water, g cm^{-3}
θ	Thiele modulus, dimensionless
ν	ratio of limiting current in backing layer and membrane, dimensionless
ξ_{H_2O}	electroosmotic drag coefficient of water, cm^3 mol^{-1}
ξ'_{MeOH}	electroosmotic drag coefficient of methanol, cm^3 mol^{-1}
ξ_{MeOH}	electroosmotic drag factor of methanol, dimensionless
γ	heat capacity ratio (γ_p/γ_v) dimensionless

References

[1] J.P. Meyers, J. Newman, Journal of the Electrochemical Society 149 (6) (Jun. 2002) A729–A735.
[2] I. Jeong, J. Kim, S. Pak, S.W. Nam, I. Moon, Journal of Power Sources 185 (2) (Dec. 2008) 828–837.
[3] C. Cho, Y. Kim, Y.-S. Chang, Journal of Thermal Science and Technology 4 (3) (2009) 414–423.
[4] J.P. Meyers, B. Bennett, Journal of Power Sources 196 (22) (Nov. 2011) 9473–9480.
[5] S. Kang, S.J. Lee, H. Chang, Journal of the Electrochemical Society 154 (11) (Nov. 2007) B1179–B1185.
[6] Y.-J. Chiu, T.L. Yu, Y.-C. Chung, Journal of Power Sources 196 (11) (Jun. 2011) 5053–5063.
[7] D. Ko, M. Lee, W.-H. Jang, U. Krewer, Journal of Power Sources 180 (1) (May 2008) 71–83.
[8] S.H. Seo, C.S. Lee, Applied Energy 87 (8) (Aug. 2010) 2597–2604.
[9] W. Wu, Y.-T. Lin, International Journal of Hydrogen Energy 35 (18) (Sep. 2010) 9701–9708.
[10] A. Casalegno, R. Marchesi, Journal of Power Sources 185 (1) (Oct. 2008) 318–330.
[11] P. Argyropoulos, K. Scott, W.M. Taama, Chemical Engineering Journal 73 (3) (Jun. 1999) 217–227.
[12] P. Argyropoulos, K. Scott, W.M. Taama, Chemical Engineering & Technology 23 (11) (2000) 985–995.
[13] P. Argyropoulos, K. Scott, W.M. Taama, Journal of Applied Electrochemistry 30 (8) (Aug. 2000) 899–913.
[14] K. Scott, P. Argyropoulos, W.M. Taama, Chemical Engineering Research and Design 78 (6) (Sep. 2000) 881–888.
[15] X. Li, Y. He, B. Yin, Z. Miao, X. Li, Journal of Power Sources 178 (1) (Mar. 2008) 344–352.
[16] P. Argyropoulos, K. Scott, W.M. Taama, Journal of Power Sources 79 (2) (Jun. 1999) 169–183.
[17] W. Wu, Y.-T. Lin, Industrial & Engineering Chemistry Research 49 (12) (Jun. 2010) 5725–5733.
[18] S.F.J. Flipsen, C. Spitas, Journal of Power Sources 196 (20) (Oct. 2011) 8472–8483.
[19] K. Scott, W. Taama, J. Cruickshank, Journal of Applied Electrochemistry 28 (3) (Mar. 1998) 289–297.
[20] Z.H. Wang, C.Y. Wang, Journal of the Electrochemical Society 150 (4) (Mar. 2003) A508–A519.
[21] F.P. Incropera, D.P. Dewitt, T.L. Bergman, A.S. Lavine, Fundamentals of Heat and Mass Transfer, sixth ed., John Wiley and Sons, New York, 2007.
[22] A.Z. Weber, J. Newman, Modeling Gas-Phase Transport in Polymer-Electrolyte Fuel Cells, Lawrence Berkeley National Laboratory, 17 Aug 2006.
[23] R. O'Hayre, S.-W. Cha, W. Colella, F.B. Prinz, Fuel Cell Fundamentals, John Wiley and Sons, New York, 2006.
[24] G. Lin, W. He, T. Van Nguyen, Journal of the Electrochemical Society 151 (12) (Dec. 2004) A1999–A2006.
[25] A. Parthasarathy, S. Srinivasan, A.J. Appleby, C.R. Martin, Journal of the Electrochemical Society 139 (9) (1992) 2530–2537.
[26] J.P. Meyers, J. Newman, Journal of the Electrochemical Society 149 (6) (Jun. 2002) A718–A728.
[27] Y. Zhu, S. Zieren, A. Manthiram, Chemical Communications 47 (26) (2011) 7410–7412.
[28] J. Ge, H. Liu, Journal of Power Sources 142 (1–2) (Mar. 2005) 56–69.
[29] J. Railio, P. Makinen, SPECIFIC FAN POWER – a tool for better performance of air handling systems, in: Proceedings of Clima 2007 WellBeing Indoors, 2007.
[30] C.L. Yaws, Handbook of Transport Property Data: Viscosity, Thermal Conductivity, and Diffusion Coefficients of Liquids and Gases, Gulf Publishing Co., Houston, TX, 1995.
[31] P.S. Kauranen, E. Skou, Journal of Applied Electrochemistry 26 (9) (Sep. 1996) 909–917.
[32] T.A. Zawodzinski, J. Davey, J. Valerio, S. Gottesfeld, Electrochimica Acta 40 (3) (Feb. 1995) 297–302.
[33] A. Havranek, K. Wippermann, Journal of Electroanalytical Chemistry 567 (2) (Jun. 2004) 305–315.
[34] A.P. Saab, F.H. Garzon, T.A. Zawodzinski, Journal of the Electrochemical Society 149 (12) (Dec. 2002) A1541–A1546.